Journal of Molecular Structure 1180 (2019) 251–259

Contents lists available at ScienceDirect

Journal of Molecular Structure

journal homepage: http://www.elsevier.com/locate/molstruc

Characterization and absorption properties of newly synthesized mono azo dyes: Experimental and theoretical approach

Çiğdem Karabacak Atay [a], Sevgi Özdemir Kart [b, *], Merve Gökalp [c], Özlem Tuğrul [b], Tahir Tilki [c]

[a] Mehmet Akif Ersoy University, Education Faculty, Elementary Education Department, 15030, Burdur, Turkey
[b] Department of Physics, Faculty of Arts and Sciences, Pamukkale University, Kinikli, 20017 Denizli, Turkey
[c] Süleyman Demirel University, Faculty of Science & Arts, Chemistry Department, 32260, Isparta, Turkey

ARTICLE INFO

Article history:
Received 23 July 2018
Received in revised form
29 November 2018
Accepted 30 November 2018
Available online 1 December 2018

Keywords:
Mono azo dyes
Pyrazole
Absorption properties
Quantum-chemical calculations

ABSTRACT

New mono azo dyes 5-amino-4-[4-(dimethylamino)phenyl]diazenyl]-pyrazol-3-ol (**A**) and 5-amino-4-[4-(dimethylamino)phenyl]diazenyl]-2-phenyl-pyrazol-3-one (**B**) are synthesized and their FT-IR, ^{1}H NMR and UV–Vis properties are measured. Computational quantum chemistry simulations based on Density Functional Theory (DFT) and Hartree-Fock (HF) by utilizing the basis set of 6-31G(d) are carried out to investigate the molecular structure and some spectroscopic properties, such as FT-IR, ^{1}H NMR,^{13}C NMR and UV–Vis spectra and the frontier molecular orbitals of Compounds **A** and **B**. Potential energy distribution (PED) is used to determine the FT-IR vibrational modes of the mono azo compounds. The correlations between the measured and calculated vibrational frequencies are found to be in good agreement with each other. UV–Vis spectrum in different solvents are measured and supported by their ab-initio calculations. The frontier molecular analysis are considered to get the electronic properties of two molecules. A good agreement between the experiment and computation results indicates that DFT and HF methods are able to provide satisfactory results for structural, spectroscopic and electronic properties of mono azo dyes.

1. Introduction

Azo dyes are organic compounds containing the coloring azo function (-N=N-) which is bound to aromatic ring. Recently, these chemical materials have received more attentions in both of the scientific and technological points of view. Azo dyes are widely utilized as a synthesized industrial organic dyes. Their industrial applications show extensive range such as sensitized solar cells [1], non-linear optical systems [2], metallochromic indicators [3], sensors [4], photochromic materials [5], liquid crystalline display [6], photo-sensitizers [7], biological-medical studies [8] and electro-optical devices and inkjet printers [9]. Additionally, azo dyes are used in dyeing textile fibers such as cotton, silk, wool, viscose and synthetic fibers [10]. These chemical materials are easy to use and to provide clear and strong colors. They are also relatively cheap materials. Azo dyes chemical materials have potential applications of antibacterial, antifungal, antitumor, antioxidant activities points of medical and pharmacology [11–13]. It is known that there is a proton tautomerization process in the structures of azo dyes, leading to their unique photo-physical and photo-chemical properties [14]. Although there are many studies on azo dye materials, it is more necessary to synthesize and characterize them by using both experimental techniques and theoretical methods to clarify some structural, spectroscopic and electronic properties of newly synthesized azo dye materials. Quantum chemical computational methods [15–18] are very powerful tools to identify and illuminate the structural, vibrational and electronic properties of the materials. Experimental data can be reinforced with the theoretical calculations with reasonable accuracy. At this point, the reliability of experimental studies or findings is increasing when the theoretical methods are supported to results. Interest in theoretical studies is increasing daily for these reasons. In our previous works [19–21], we have investigated the structural and spectroscopic properties of some disazo and mono azo dyes by using quantum chemical computational methods. Sener et al. [22] have synthesized disazo dyes with pyrazole skeleton and characterized their structures and spectroscopic properties by using experimental

* Corresponding author.
E-mail address: ozsev@pau.edu.tr (S.Ö. Kart).

https://doi.org/10.1016/j.molstruc.2018.11.108
0022-2860/

characterization techniques such as FT-IR, ^{1}H NMR and theoretical approach. Yıldırım et al. [23] have synthesized new coumarin based disazo dyes and clarified their structural and spectroscopic properties by experimental techniques as well as theoretical quantum computational methods.

The main aim of the present work is to investigate the structural and spectroscopic properties of two newly synthesized mono azo dyes (Molecule **A** and **B**) by performing experimental techniques and quantum computational methods based on DFT and HF. FT-IR and ^{1}H NMR spectra of new mono azo dyes are measured in order to obtain the chemical structure and vibrational properties. The molecular structural parameters such as bond length, bond angle bond dihedral angles, fundamental vibrational modes, ^{1}H NMR, ^{13}C NMR and UV–Vis spectra and molecular orbitals of the mono azo dyes compounds considered in this study are identified by performing quantum chemical computations. Absorption spectra of two molecules are observed to obtain the wavelength at the maximum absorption of UV–Vis wave.

This work is organized as follows: the experimental details are introduced in Section 2. The computational quantum chemistry methods we follow are presented in Section 3. The results of structural and some spectroscopic properties for two molecules obtained from experiment and ab-initio simulations are presented and discussed in Section 4. Moreover, the observed data are compared with their theoretical values in the same section. Finally, the last Section 5 of this work deals with the conclusion arising from the main results.

2. Experimental method

2.1. Synthesis of 5-amino-4-[4-(dimethylamino)phenyl]diazenyl]-pyrazol-3-ol (A)

10 ml hydrochloric acid is added to 0.02 mol N,N-dimethyl-*p*-phenylenediamine and the mixture is magnetically stirred at 0–5 °C in a salt-ice bath. 1.4 g $NaNO_2$ (in 5 ml water) is added dropwise to the solution over 1 h and the diazonium salt is formed. In another beaker, the coupling compound is prepared by adding 1.2 g Na_2CO_3 + 0.4 g NaOH solutions (in water) at 0–5 °C onto 0.02 mol of 3-amino-5-hydroxypyrazole. After diazotization, the prepared diazonium salt is added dropwise to the coupling agent and is continued to be magnetically stirred in a salt-ice bath at 0–5 °C for 4 h. The mixture is adjusted to pH 6 at room temperature, stirred, filtered with cold water in vacuum and crystallized in appropriate solvent mixtures.

2.2. Synthesis of 5-amino-4-[4-(dimethylamino)phenyl]diazenyl]-2-phenyl-pyrazol-3-one (B)

5-amino-4-[4-(dimethylamino)phenyl]diazenyl]-2-phenyl-pyrazol-3-one **(B)** is synthesized by following the procedure of 5-amino-4-[4-(dimethylamino)phenyl]diazenyl]-pyrazol-3-ol **(A)**. However, instead of 3-amino-5-hydroxypyrazole, 3-amino-1-phenyl-2-pyrazolin-5-one is used as a coupling agent in the synthesis of compound **B**.

The synthesis schemes of compounds **A** and **B** are shown in Fig. 1.

2.3. Experimental equipment

IR spectra are recorded on a Schimadzu IR Prestige-21 Fourier Transform-infrared (FT-IR) spectrophotometer. Nuclear magnetic resonance spectra for the compound **A** and **B** are measured by using Bruker Avance 125 MHz. All of the wavenumbers are recorded via Schimadzu UV-1601 double beam spectrophotometer. Melting points for the compounds are utilized by Smart SMP30 Stuart melting point apparatus.

3. Computational method

Quantum chemistry calculations are carried by using DFT and HF methods implemented in the Gaussian 09 Package Program [24,25] in order to get the information about structural and vibrational frequencies of the mono azo dyes. 6-31G (d) basis set is used to represent the electronic wave function in the DFT and HF in order to turn the partial differential equations of the model into algebraic equations suitable for efficient implementation on a computer. Molecular structures of the mono azo dyes are optimized to reach the global minima at the level of ab-initio chemistry methods based on DFT within B3LYP (which stands for Becke, 3-parameter, Lee-Yang-Parr) and HF by considering C1-symmetry.

The optimized molecular structures of the Molecule **A** and **B** are demonstrated in Fig. 2 (a) and (b) with the atomic numbering. The same basis set and computational methods with those utilized in the optimization are used to predict the vibrational frequencies of azo dyes molecules of the optimized structures. ^{1}H NMR and ^{13}C NMR shielding constants are also calculated by applying the Gauge-Including Atomic Orbitals (GIAO) implemented in DFT and HF methods [25] in the solvents of chloroform, acetic acid, methanol, dimethylformamide (DMF) and dimethylsulphoxide (DMSO). The ^{1}H NMR and ^{13}C NMR chemical shift computations are analyzed by taking into account the Tetramethylsilane (TMS) as a reference. Wavenumber calculations verify the stability of the optimized geometries, giving positive values for all the computed wavenumbers. Vibrational Energy Distribution Analysis program (VEDA 4) [26] is used to calculate Potential Energy Distribution (PED) for each of the vibrational frequencies. PED calculations show the relative contribution of the internal coordinates to each normal vibrational mode of the molecules. Thus, the character of each mode can be described. The PEDs for the assignments of the experimental bands clarify the fundamental vibrational modes. The vibrational frequencies predicted from computational quantum chemistry methods are multiplied by the appropriate scaled factors [27] to compare with those obtained from experiments. The incomplete incorporation of electron correlation and the use of finite basis set in simulations give rise to some systematic errors. Hence, the scaled factors such as 0.9614 and 0.8953 for DFT and HF computational methods [27] are considered for determining the accurate vibrational spectra of the molecules. The values of the vibrational frequency modes obtained from DFT and HF for the optimized geometry of the title molecules are collected in Table 2, along with the corresponding experimental data.

UV–vis spectrum analyses of azo dyes considered in this work are accomplished by using Time Dependent Density Functional Theory (TD-DFT) employing B3LYP level with the basis set of 6-31G(d) in five different solvents, such as chloroform, acetic acid, methanol, dimethylformamide (DMF) and dimethylsulphoxide (DMSO).

4. Results and discussion

4.1. Molecular geometry

The geometric structures of the Molecules **A** and **B** calculated from DFT and HF methods are represented in Fig. 2 (a) and (b), along with the atom numbering schemes, respectively. The geometry of the molecules possesses C_1 point group symmetry. These molecules have got 32 and 42 atoms and possess 90 and 120 fundamental vibrational modes, respectively. Molecule **A** consists of 11 C atoms, 6 N atoms, 14 H atoms and 1 O atom. On the other

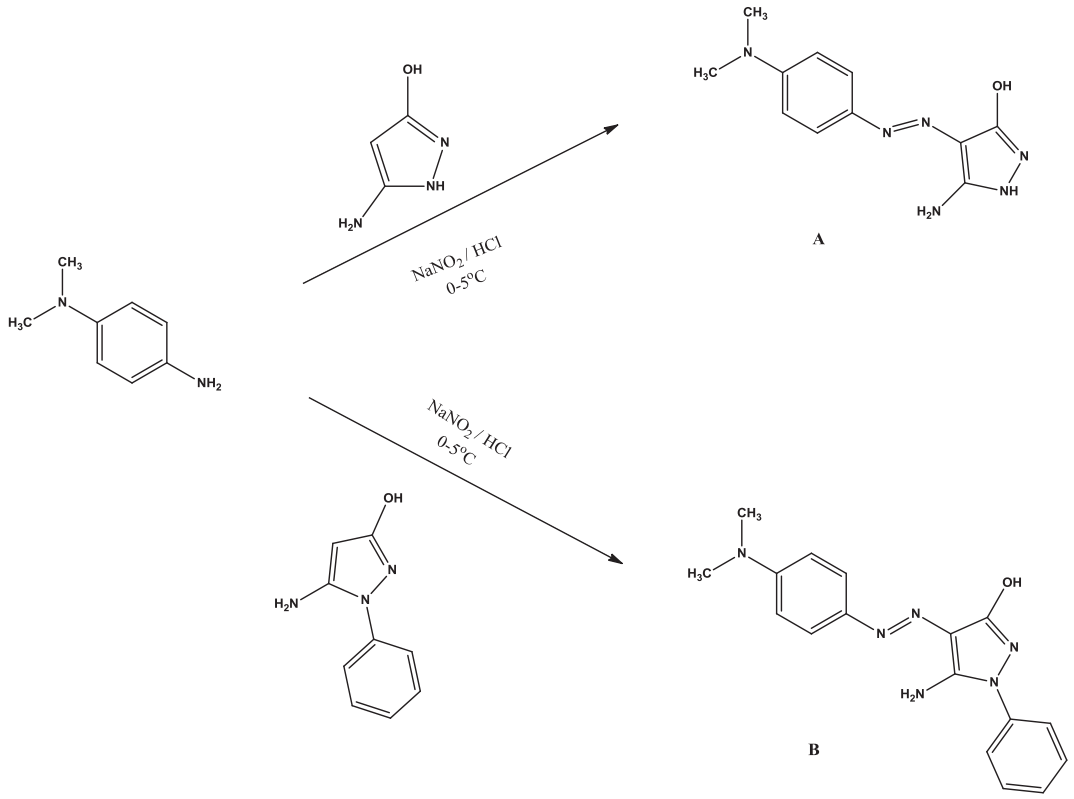

Fig. 1. The synthetic scheme for the preparation of Compounds **A** and **B.**

hand, 17 C atoms, 7 N atoms 18 H atoms and 1 O atom constitute Molecule **B**. The main difference in the structure of Molecule **A** with Molecule **B** is the presence of benzene ring (Fig. 2b) in Molecule **B** instead of 29 H atom shown in Fig. 2a.

4.2. Structural properties

The structural parameters of the bond length, bond angle and dihedral angle of the molecule **A** and **B** determined from DFT and HF methods are presented in Tables S1 and S2 as a supplementary material, respectively. In order to define the molecular structure of the molecule **A**, 33 bond lengths, 52 bond angles and 67 dihedral angles are necessary. As we interest in the molecule B, 44 bond lengths, 70 bond angles and 95 dihedral angles constitute the structure. These bond lengths, bond angles and dihedral angles given in the Tables S1 and S2 are shown in Fig. 2 (a) and (b). The results computed from two methods are almost close to each other. To the best of our knowledge, experimental data on the geometric structure of the mono azo dyes molecules considered in this study are not available in the literature. Tables S1 and S2 show that when the benzene ring is substituted for 29 H atom in Molecule A, the lengths for C–N and C–O bonds decrease while the other bonds do not change significantly. When analyzing the bond angles of the molecules, there is no difference in distant region, while the changes in the angles between atoms near the benzene ring are recorded.

4.3. Keto-enol tautomerization

Tautomerism is related by the migration of an atom, usually a hydrogen atom varying from one side of molecule to another side. Each of tautomer has different properties. The most common tautomer is the keto-enol tautomer that is formed via a movement of hydrogen atom from carbon to oxygen. The keto-enol tautomerism is also observed in **A** and **B** molecules synthesized in this work and the tautomeric forms of compounds **A** and **B** are presented in Fig. 3.

4.4. Analysis of vibrational spectra

The infrared spectroscopy provides information about the molecular structure and interactions within the sample. This spectroscopy technique is not destructive and invasive tool. It measures vibrational energy associated with the chemical bonds in a sample. The vibrational spectrum is used as like fingerprint to identify and characterize the structure of the chemical materials.

In this work, the theoretical and experimental vibrational frequencies data of the synthesized molecules are obtained to reach the spectroscopic signature of the compounds. **A** and **B** molecules consist of 32 and 42 atoms, respectively. Moreover, they vibrate under 90 and 120 normal modes, respectively. The vibrational spectra of FT-IR calculated by using DFT method utilizing 6-31G(d) basis set and experimentally are plotted in Figure S1 (a), (b), (c) and (d) for the Compound **A** and **B**, respectively, as supplementary materials.

The Compound **A** has 90 vibrational normal modes: 31 modes are stretching vibration, 30 modes are bending vibrations and the others 29 modes are torsional vibration modes. Additionally, 30 CH modes take part in the vibrational behavior. As for the Compound **B** is considered, 120 fundamental modes are constituted: 41 modes are stretching, 40 modes are bending and the rest (39 modes) are torsional modes. This molecule includes 45 CH modes. The results of FT-IR calculations are consistent with those of the experimental data after applying the scale factors to the theoretical values, as seen in Tables S3 and S4 provided as supplementary materials.

It is important to handle some fundamental vibrational modes

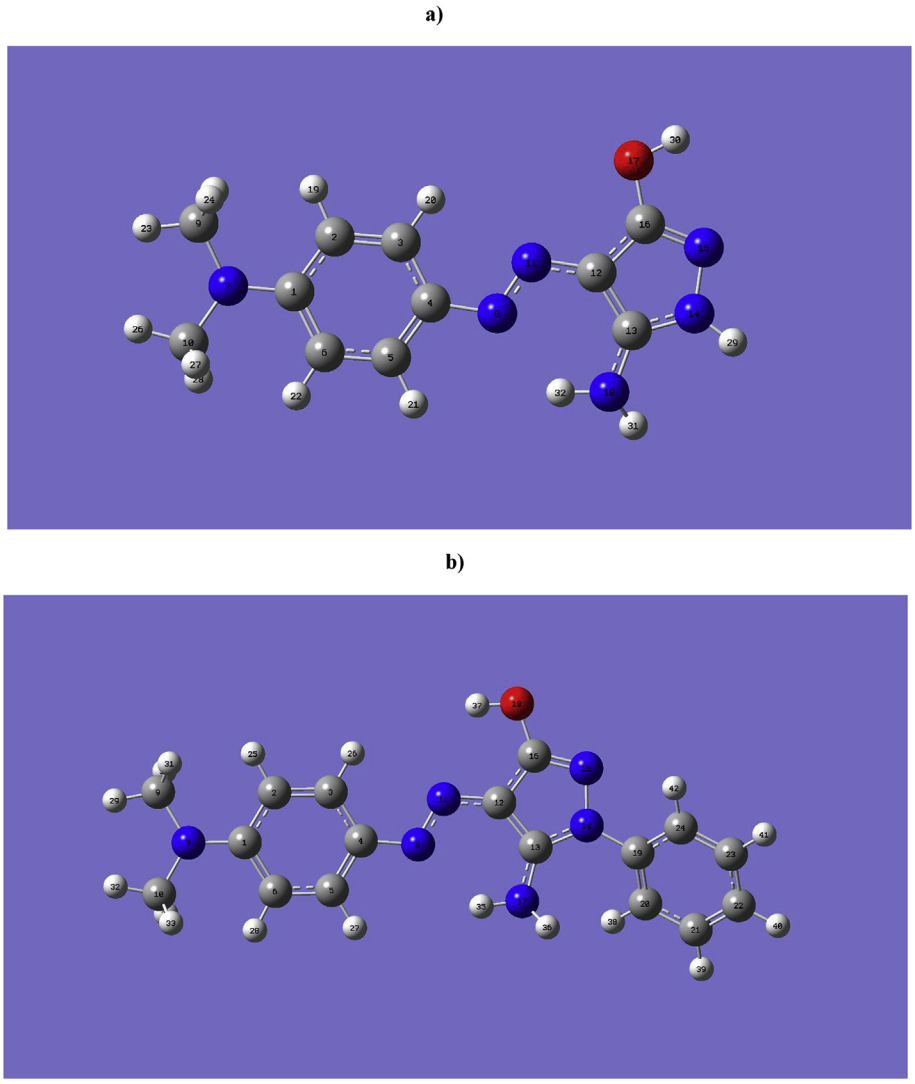

Fig. 2. The optimized structures of Compounds **A (a)** and **B (b)** with the atomic numbering scheme, respectively.

Table 1
Comparison of the experimental data and theoretical FT-IR values obtained from DFT and HF methods for X–H (X:O, N), Ar–H, Alip-H, N=N groups in **A** and **B** molecules.

	Experimental				FT-IR (cm^{-1}) DFT/B3LYP/6-31G(d)				HF/6-31G(d)			
	ν_{X-H}	ν_{Ar-H}	ν_{Alip-H}	$\nu_{N=N}$	ν_{X-H}	ν_{Ar-H}	ν_{Alip-H}	$\nu_{N=N}$	ν_{X-H}	ν_{Ar-H}	ν_{Alip-H}	$\nu_{N=N}$
Compound A	3360 (OH)	2880	2360	1520	3572 (OH)	3108	3031	1441	3652 (OH)	3060	2975	1465
	3150 (NH)	2790			3328 (NH)		2949		3440 (NH)		2891	
Compound B	3440 (OH)	3200	3000	1500	3543 (OH)	3106	3034	1439	3657 (OH)	3059	2972	1451
	3300 (NH)	3120	2740		3481 (NH)	3099	2951		3504 (NH)	3046	2922	

Table 2
Comparison of experimental ^{1}H NMR chemical shifts and the theoretical corresponding values calculated from DFT and HF methods for Alip-H, Aro-H, X–H (X:O,N) groups in **A** and **B** molecules.

Experiment				^{1}H NMR (d, ppm, DMSO-d_6) DFT/B3LYP			HF		
	Alip-H	Aro-H	X–H	Alip-H	Aro-H	X–H	Alip-H	Aro-H	X–H
Compound A	2.90 (d. 6H CH_3)	5.69–7.37 (m. 4H)	10.31 (NH_2) 12.86 (OH)	2.46–2.96 (d. 6H CH_3)	6.23–7.29 (m. 4H)	3.05–6.43 (NH_2) 4.43 (OH)	2.17–2.55 (d. 6H CH_3)	6.19–7.75 (m. 4H)	3.08–6.16 (NH_2) 4.82 (OH)
Compound B	2.93 (d. 6H CH_3)	6.23–7.94 (m. 9H)	13.18 (NH_2)	2.50–2.96 (d. 6H CH_3)	6.23–7.33 (m. 9H)	3.43–6.39 (NH_2) 5.62 (OH)	2.19–2.55 (d. 6H CH_3)	6.22–7.41 (m. 9H)	3.48–6.21 (NH_2) 5.81 (OH)

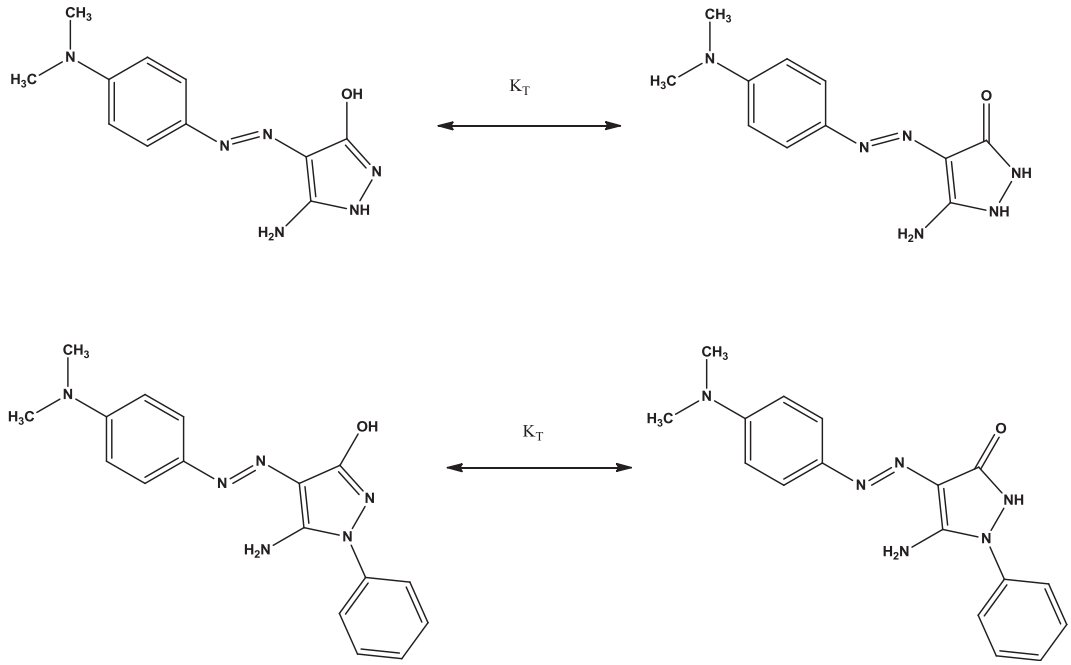

Fig. 3. Tautomeric forms of Compounds **A** and **B.**

observed in the Compounds **A** and **B**. Table 1 presents some significant assigned fundamental vibrational modes computed from DFT and HF methods. The corresponding experimental results are also listed in Table 1 to compare them with the theoretical results. The vibrational wavenumbers and IR intensity calculated from DFT and HF, and the assignments of IR vibration modes for the title compounds are given in Tables S3 and S4, as supplementary materials.

The FT-IR spectrum of Compound **A** shows that −OH, −NH, aromatic (Ar−H) and aliphatic (Alip-H) bands are observed at 3360 cm^{-1}, 3150 cm^{-1}, 2880-2790 cm^{-1} and 2360 cm^{-1}, respectively. The corresponding DFT/B3LYP predictions of these bands are obtained as 3572 cm^{-1}, 3328 cm^{-1}, 3108 cm^{-1} and 3031-2949 cm^{-1}, respectively. These four bands are evaluated as 3652 cm^{-1}, 3440 cm^{-1}, 3060 cm^{-1} and 2975-2891 cm^{-1} by using the HF method, correspondingly. The FT-IR spectra of azo (N=N) band is measured as the value of 1520 cm^{-1} and it is calculated as 1441 cm^{-1} (DFT) 1465 cm^{-1} (HF). On the other hand, the FT-IR spectra of **B** compound shows −OH band at 3440 cm^{-1},−NH band at 3300 cm^{-1}, aromatic (Ar−H) band at 3200-3120 cm^{-1} and aliphatic (Alip-H) band at 3000-2740 cm^{-1}. The predictions by DFT method for −OH, −NH band, aromatic (Ar−H) and aliphatic (Alip-H) bands are calculated as 3543 cm^{-1}, 3481 cm^{-1}, 3106-3099 cm^{-1}, 3034-2951 cm^{-1}, respectively, while those by HF method for are founded as 3657 cm^{-1}, 3504 cm^{-1}, 3059-3046 cm^{-1} and 2972-2922 cm^{-1}, respectively. The FT-IR spectrum of azo (N=N) band measured as 1500 cm^{-1} is confirmed by its ab-initio calculations predicted as 1439 cm^{-1} (DFT) and 1451 cm^{-1} (HF). When the 29 H atom in Molecule **A** is replaced by benzene ring, the vibrational frequencies of the N−H and O−H bands are increased, those of N=N and O−H bands do not chance much in the calculations.

Linear regressions between the experiment and computations are fulfilled by using the linear equation of $y = Ax + B$, where A and B are fit constants. The correlations between the experimental and theoretical frequencies calculated from DFT/B3LYP for Compound **A** and **B** are linear, as shown in Figure S2 (a) and Figure S3 (a) as supplementary materials. The fitting parameters are given in the following equalities: $y = 0.8460x + 219.0989$ ($R^2 = 0.9091$) and $y = 0.8394x + 230.9081$ ($R^2 = 0.9384$), respectively. The linear regression between the experiment and the calculation by HF method are also illustrated for **A** and **B** molecules in Figure S2 (b) and Figure S3 (b) as supplementary materials, respectively. The results of FT-IR calculated from HF method for Compound **A** and **B** are more convenient with the measured values than those by DFT method, as shown in the following equations: $y = 0.8460x + 182.4846$ ($R^2 = 0.9695$) and $y = 0.8981x + 255.6069$ ($R^2 = 0.9515$), respectively.

4.5. NMR spectra

The use of ^1H and ^{13}C NMR spectroscopies allows ones to characterize the structures of **A** and **B** molecules further. The ^1H NMR spectra of the Compound **A** and **B** are measured in the medium of DMSO. ^1H NMR spectra observed for both molecules are given in Fig. 4. The Compound **A** shows broad peaks at 10.31 ppm (NH_2), and 12.86 ppm (OH) for pyrazole. Moreover, the other chemical shift values of 7.37−5.69 ppm (aromatic H) and 2.90 ppm (aliphatic H) are recorded. As for the Compound **B,** the main peaks are placed at 13.18 ppm, 7.94−6.23 ppm and 2.93 ppm for the pyrozoles of NH_2, aromatic H and aliphatic H, respectively.

^1H and ^{13}C chemical shift calculations based on GIAO-DFT and GIAO-HF methods with respect to TMS are performed in the medium of DMSO. Our simulation results of the ^1H chemical shift values for the Compounds **A** and **B** are listed in the Table 2, along with the corresponding experimental data. As seen in Table 2, experimental chemical shift values of aromatic and aliphatic groups are compatible with the theoretical chemical shifts, except for those of NH_2 and OH peaks which resonate at different regions because of tautomerization. The ^1H NMR calculated from both DFT/B3LYP and HF methods for the Molecules **A** and **B** are provided in Table S5 along with the experimental data, as a supplementary material. For Molecule **A**, ^{13}C NMR chemical shift values computed by DFT/B3LYP and HF. The ^{13}C NMR values computed from HF method are indicated by parentheses next to the data calculated from DFT method. 133.64 (134.42), 98.98 (90.95), 101.36 (101.18), 128.88 (120.37), 117.00 (115.43) and 97.92 (90.21) ppm are

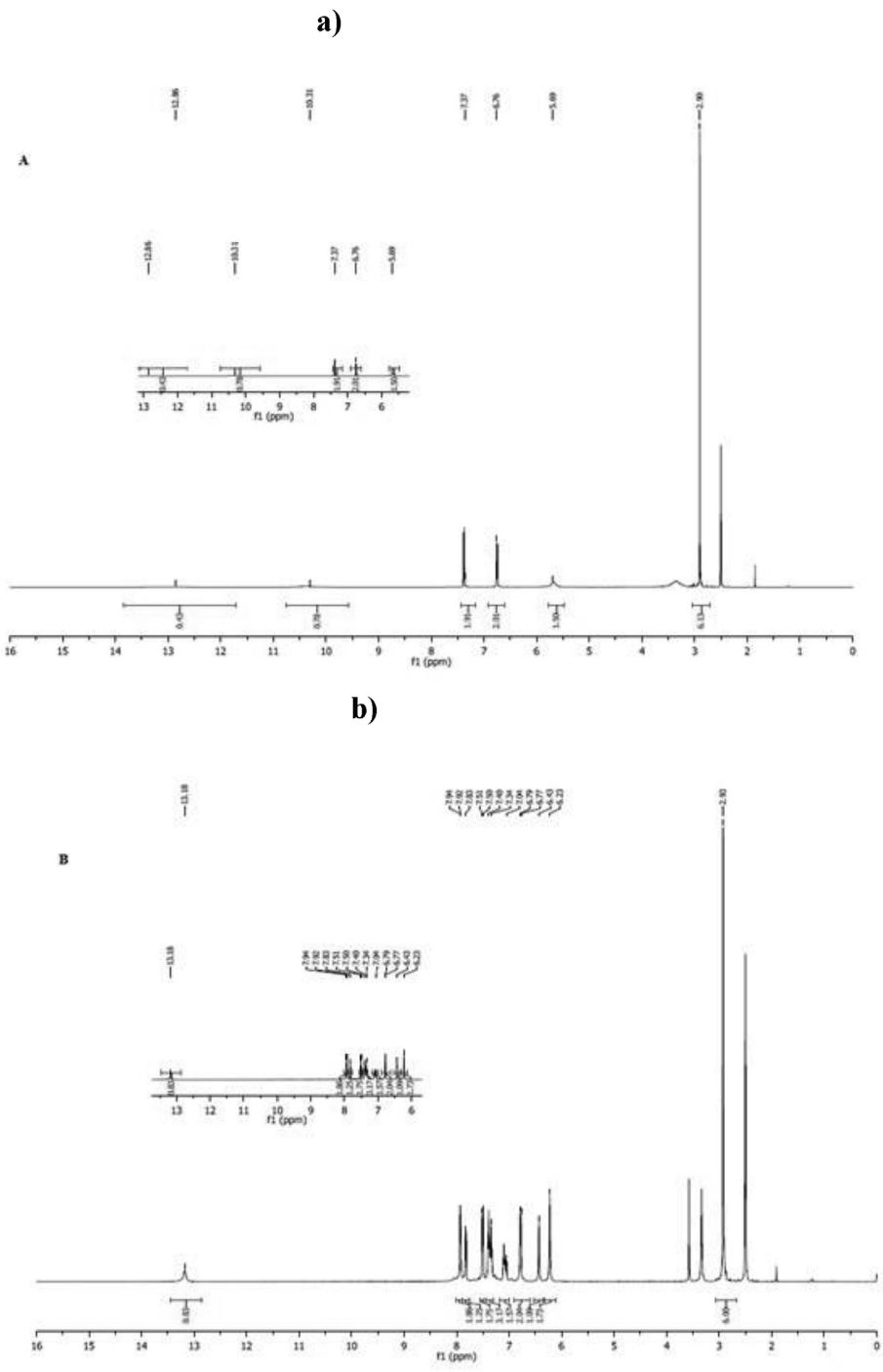

Fig. 4. The experimental ^{1}H NMR spectrum for a) Compound **A** and b) Compound **B**.

dedicated to phenyl carbons (C1–C6), as listed in Table S6, as a supplementary material. Additionally, pyrazole carbons (C12, C13 and C16) and methyl carbons (C9 and C10) are resonated at 100.23 (85.66), 125.52 (131.26), 142.68 (144.12), 32.44 (20.35), 32.53 (20.39) ppm, respectively. As for Molecule **B**, the chemical shifts of 133.78 (134.88), 99.02 (90.56), 101.04 (101.19), 128.34 (119.59), 117.68 (116.33) and 97.82 (89.86) ppm are contributed by phenyl carbons (C1–C6). Furthermore, the resonances of 101.90 (86.78), 123.06 (129.10) and 144.24 (144.62) ppm are attributed to the pyrazole carbons (C12, C13 and C16). The phenyl carbons bonded to the pyrozole ring are resonated at 125.14 (121.26), 104.48 (100.41), 115.36 (111.72), 111.67 (106.94), 116.27 (112.61) and 108.64 (103.76) ppm is also dedicated to phenyl carbons which bonded to the pyrazole ring while 32.54 (20.37) and 32.43 (20.40) ppm are assigned to methyl carbons (C9 and C10).

4.6. UV–vis spectra

UV–Vis spectrophotometer uses visible and ultraviolet light to characterize the structure of chemical material. It is used to measure the wavelength of light absorbed via compound. Therefore, this technique provides molecular structure of a compound as well

as the related information. UV–Vis absorption spectra obtained by experiment and TD-DFT computations are presented in Fig. 5. As we see in, the experimental absorbance spectra show a main peak at different wavelength for five different solvents with different polarities (methanol, acetic acid, dimethylsulphoxide, chloroform and dimethylformamide), while the effect of solvents on the wavelength at the maximum absorbance (λ_{max}) are not displayed significantly.

When the UV spectrum of Molecule **A** is examined, two maximum absorption bands are observed in all solvents except methanol. It has been found that the first λ_{max} values of DMSO and acetic acid show more bathochromic shifts and the corresponding value of DMF is more hypsochromic shift than that of chloroform. On the other hand, the second λ_{max} value of acidic acid shows more bathochromic shift, while those of the rest present more hypsochromic shifts than that of chloroform. As dealt with Compound B, although a double maximum is observed in acetic acid and chloroform, the spectrum display a single peak in the solvents of DMSO, DMF and methanol. The hypsochromic shifts are dominant in all solvents except for chloroform. As we are interested in the wavelengths of the first maxima, chloroform shows more bathochromic shift than acetic acid.

The results of λ_{max} computed from TD-DFT for Compound **A** and **B** in the different solvents are given in Table 3, where they are compared with those of experiment. The ab-initio results are in good agreement with those of experiment, as seen in Table 3. It revealed that from the table that Molecule **A** and **B** absorb light at the wavelength of about 410 nm and 430 nm, respectively.

4.7. Frontier molecular orbital (FMOs) analysis

Molecular orbitals (HOMO-LUMO) and their energies are very important parameters for quantum chemistry. They can also provide an important insight into workings of organic reactions and controlling the outcome of reactions [28]. HOMO and LUMO stand for the highest occupied molecular orbital and the lowest unoccupied molecular orbital, respectively. The energy difference between the HOMO and LUMO molecular orbital is called as HOMO-LUMO band gap, an important value for the stability condition for the compounds. HOMO and LUMO acronyms are known as the frontier molecular orbitals (FMOs) and they also play an important role in determining the optical and electrical properties of molecules. HOMO represents the ability to donate an electron, while LUMO corresponds the ability to receive an electron. To investigate the energetic behavior and the stability of the Compounds **A** and **B**, the electronic calculations are carried out by using both DFT and HF methods. The HOMO-LUMO energy gaps computed from DFT method for both compounds are shown in Fig. 6. Table 4 presents total energies, HOMO and LUMO energies, HOMO-LUMO band gaps (ΔE) and dipole moments (μ) predicted by DFT and HF methods. LUMO energies calculated from DFT for the Compounds **A** and **B** are −1.2817 eV and −1.5864 eV in gas phases, respectively. HOMO energies predicted from DFT method for the Chemical materials **A** and **B** are found as −4.6939 eV and −4.8382 eV, respectively. The energy gaps of the HOMO-LUMO for the Compounds **A** and **B** are calculated as −3.4150 eV and −3.2518 eV by using DFT method, as shown in Fig. 6.

The energy gap of HOMO-LUMO explains the eventual charge

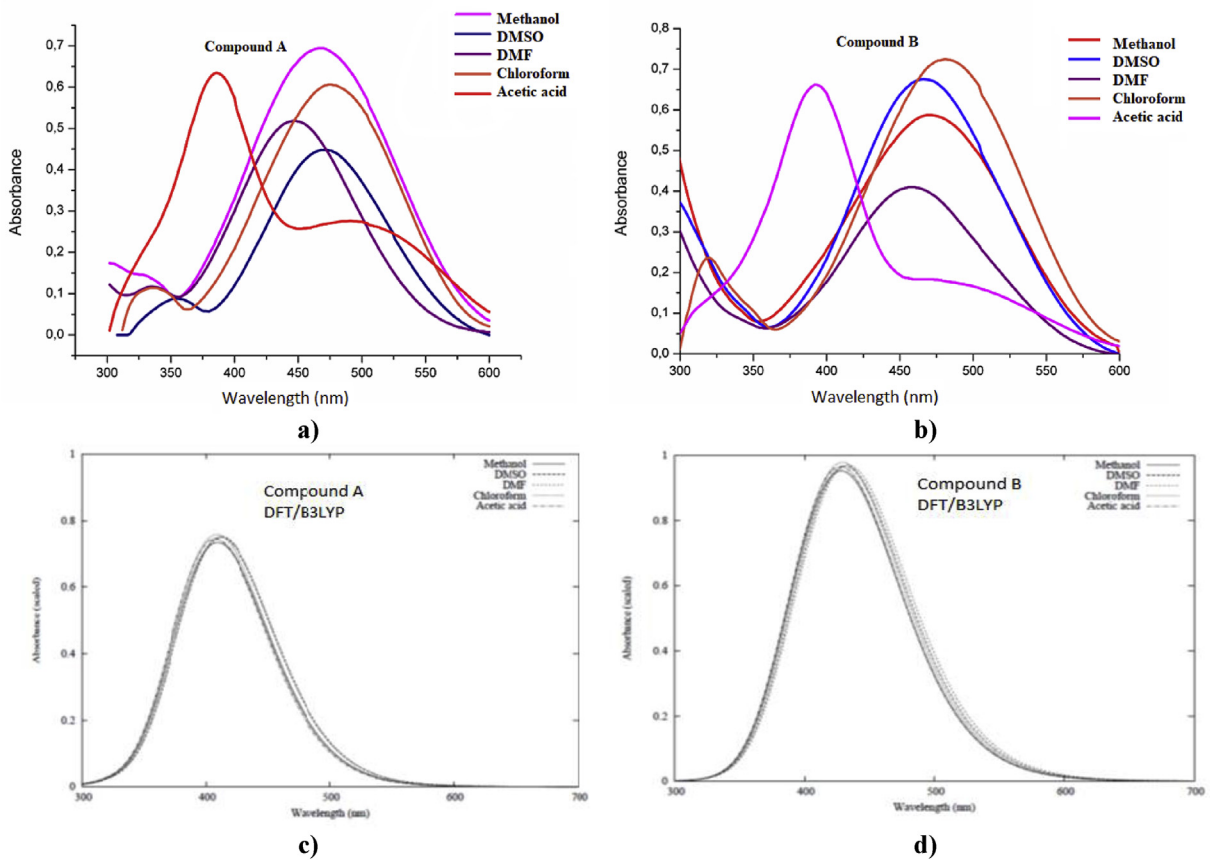

Fig. 5. The experimental and theoretical (predicted by using DFT/B3LYP) absorption spectrum (UV–vis) of Compounds **A** and **B** in the five different solvents of methanol, DMSO, DMF, chloroform and acetic acid.

Table 3
The wavelength representing maximum absorbance λ_{max} (nm) calculated by DFT/B3LYP method for the Compound **A** and **B** in the solvents of DMSO, DMF, methanol, acetic acid and chloroform, compared with corresponding experimental results.

	λ_{max} (nm)									
	Experiment					DFT calculations				
	DMSO	DMF	Methanol	Acetic Acid	Chloroform	DMSO	DMF	Methanol	Acetic Acid	Chloroform
Compound A	472–356	448–336	470	492–386	476–338	413	413	410	409	409
Compound B	466	460	472	470–392	482–320	432	434	429	428	430

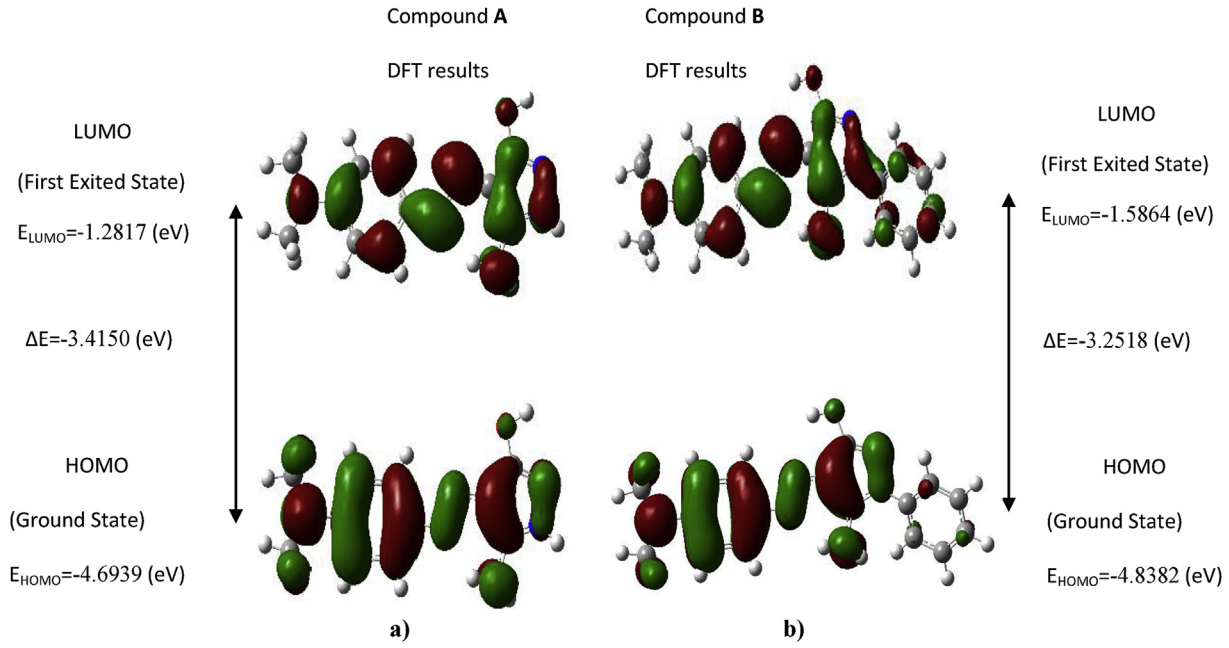

Fig. 6. The schema displaying the frontier molecular orbitals (HOMO and LUMO) computed via DFT/B3LYP method in the gas phase for a) Compound **A** and b) Compound **B**.

Table 4
The energy values E (eV), HOMO-LUMO gap energy Δ*E* (eV) and dipole moment μ (*D*) calculated from DFT and HF methods for Compounds **A** and **B.**

	Compound A		Compound B	
	DFT	HF	DFT	HF
E_{total} (eV)	−22619.7151	−22481.051	−28907.1122	−28727.3809
E_{HOMO}(eV)	−4.6939	−6.7783587	−4.8382	−7.0995
E_{LUMO} (eV)	−1.2817	−2.8735234	−1.5864	−2.3592
$\Delta E_{HOMO\text{-}LUMO\ gap}$ (eV)	−3.4150	−3.9075565	−3.2518	−9.4587
Dipol moment, μ (*D*)	3.2828	3.6215	5.8686	5.4351

transfer interaction within the molecule. The HOMO predicted for the molecule **A** is distributed on the whole molecule while LUMO is localized on the coloring azo function (-N═N-) as shown in Fig. 6 (a). As for Molecule **B** HOMO and LUMO charges are distributed on the whole molecule, as shown in Fig. 6 (b).

5. Conclusion

The structural and some spectroscopic properties of two mono azo dyes are synthesized in this work are identified by performing the measurements of FT-IR, ^{1}H NMR and UV–Vis spectra and accomplishing their ab-initio calculations based on DFT and HF methods. Solvatochromic properties of these new molecules are evaluated from their visible absorption properties displaying in the solvents of chloroform, acetic acid, methanol, DMF and DMSO. The geometries of the mono azo dyes are optimized through both DFT/B3LYP and HF methods including the basis set of 6-31G(d). The bond lengths, bond angles and dihedral angles are obtained as structural properties by employing these quantum computational methods. The fundamental vibrational modes of the mono azo dyes are assigned. The vibrational frequencies computed from DFT and HF methods show similar behavior with the results obtained from the experiment. The computational values of the harmonic frequencies deviate slightly from the experimental data. The disagreement between the values of computations and those of measurements may be due to neglecting of the anharmonic effects and the general tendency of the quantum chemical methods to overestimate the force constants at the equilibrium geometry. The correlation between the calculation and experimental FT-IR data is provided by fitting our data to linear equations for two molecules. It can be reported that the theoretical frequencies calculated from the DFT and HF methods are convenient with the

observed data, because the regression coefficients get approximately unity. The positions of hydrogen and carbon atoms of mono azo dyes synthesized in this study are determined by means of the computed ^{1}H and ^{13}C NMR chemical shifts as well as corresponding experimental values of ^{1}H NMR. The analysis of the UV–Vis spectrum for new mono azo dyes are performed by utilizing not only experimental methods but also quantum chemical computational methods. The observed wavelength representing the maximum absorbance in the UV–Vis spectrum varies with the solvents, while the corresponding values calculated don't show remarkable change. Our UV–Vis spectrum indicates that theoretical values of λ_{max} agree well with the experimental data. The electronic properties of two molecules are revealed by fulfilling frontier molecular analysis. To our knowledge, our results obtained experimentally and theoretically are presented in the study for the first time. It can be reported that DFT/B3LYP and HF methods with the basis set of 6-31G(d) are powerful tools to study the structural, vibrational and electronic properties of mono azo dyes chemical materials.

Acknowledgements

This study has been supported by Pamukkale University (Grant Nos: 2018KRM002-448).

Appendix A. Supplementary data

Supplementary data to this article can be found online at https://doi.org/10.1016/j.molstruc.2018.11.108.

References

[1] P. Prajongtat, S. Suramitr, S. Nokbin, K. Nakajima, K. Mitsuke, S. Hannongbua, Density functional theory study of adsorption geometries and electronic structures of azo-dye-based molecules on anatase TiO2 surface for dye-sensitized solar cell applications, J. Mol. Graph. Model. 76 (2017) 551–561. https://doi.org/10.1016/j.jmgm.2017.06.002.

[2] F. Borbone, A. Carella, L. Ricciotti, A. Tuzi, A. Roviello, A. Barsella, High nonlinear optical response in 4-chlorothiazole-based azo dyes, Dyes Pigments 88 (2011) 290–295. https://doi.org/10.1016/j.dyepig.2010.07.011.

[3] C. Woodward, H. Freiser, Sulphonated azo-dyes as extractive metallochromic reagents, Talanta 20v (1973) 417–420. https://doi.org/10.1016/0039-9140(73)80172-9.

[4] F.L. Coelho, C. de Á. Braga, G.M. Zanotto, E.S. Gil, L.F. Campo, P.F.B. Gonçalves, F.S. Rodembusch, F.S. Santos, Low pH optical sensor based on benzothiazole azo dyes, Sensor. Actuator. B Chem. 259 (2018) 514–525. https://doi.org/10.1016/j.snb.2017.12.097.

[5] N.O. Mahmoodi, S. Rahimi, M.P. Nadamani, Microwave-assisted synthesis and photochromic properties of new azo-imidazoles, Dyes Pigments 143 (2017) 387–392. https://doi.org/10.1016/j.dyepig.2017.04.053.

[6] D.D. Huang, E.P. Pozhidaev, V.G. Chigrinov, H. L Cheung, Y. L Ho, H. S Kwok, Photo-aligned ferroelectric liquid crystal displays based on azo-dye layers, Displays 25 (2004) 21–29. https://doi.org/10.1016/j.displa.2004.04.003.

[7] K.J. AL-Adilee, A.K. Abass, A.M. Taher, Synthesis of some transition metal complexes with new heterocyclic thiazolyl azo dye and their uses as sensitizers in photo reactions, J. Mol. Struct. 1108 (2016) 378–397. https://doi.org/10.1016/j.molstruc.2015.11.038.

[8] A.Z. El-Sonbati, M.A. Diab, A.A. El-Bindary, A.F. Shoair, M.A. Hussein, R.A. El-Boz, Spectroscopic, thermal, catalytic and biological studies of Cu(II) azo dye complexes, J. Mol. Struct. 1141 (2017) 186–203. https://doi.org/10.1016/j.molstruc.2017.03.082.

[9] S. Kiani, M.S. Zakerhamidi, H. Tajalli, Hydrogen bonding intermolecular effect on electro-optical response of doped 6PCH nematic liquid crystal with some azo dyes, Opt. Mater. 55 (2016) 121–129. https://doi.org/10.1016/j.optmat.2016.03.019.

[10] X. Chen, Q. Deng, S. Lin, C. Du, S. Zhao, Y. Hu, Z. Yang, Y. Lyu, J. Han, A new approach for risk assessment of aggregate dermal exposure to banned azo dyes in textiles, Regul. Toxicol. Pharmacol. 91 (2017) 173–178. https://doi.org/10.1016/j.yrtph.2017.10.022.

[11] H. Khanmohammadi, V. Arab, K. Rezaeian, G.R. Talei, M. Pass, N. Shabani, Diaminomaleonitrile-based azo receptors: Synthesis, DFT studies and their antibacterial activities, J. Mol. Struct. 1129 (2017) 169–178. https://doi.org/10.1016/j.molstruc.2016.09.071.

[12] A. Mohammadi, B. Khalili, M. Tahavor, Novel push–pull heterocyclic azo disperse dyes containing piperazine moiety: Synthesis, spectral properties, antioxidant activity and dyeing performance on polyester fibers, Spectrochim. Acta 150 (2015) 799–805. https://doi.org/10.1016/j.saa.2015.06.024.

[13] M.A. Gouda, H. Fakhr, E. Margret, M. Girges, M.A. Berghot, Synthesis and antitumor evaluation of thiophene based azo dyes incorporating pyrazolone moiety, J. Saudi Chem. Soc. 20 (2016) 151–157. https://doi.org/10.1016/j.jscs.2012.06.004.

[14] A.G. Gilani, V. Taghvaei, E.M. Rufchahi, M. Mirzaei, Photo-physical and structural studies of some synthesized arylazoquinoline dyes, Spectrochim. Acta 185 (2017) 111–124. https://doi.org/10.1016/j.saa.2017.05.035.

[15] K.I. Ramachandran, G. Deepa, K. Namboori, Computational Chemistry and Molecular Modelling: principles and applications, Springer-Verlag Berlin Heidelberg, 2008.

[16] F. Jensen, Introduction to Computational Chemistry, 2nd Edition, John Wiley & Sons Ltd, 2007.

[17] C.J. Cramer, Essentials of Computational Chemistry: theories and models, John Wiley & Sons Ltd, 2004.

[18] E.G. Lewars, Computational Chemistry:Introduction to the Theory and Applications of Molecular and Quantum Mechanics, Edition, vol. 3, Springer, 2016.

[19] Ç. Karabacak, O. Dilek, Synthesis, solvatochromic properties and theoretical calculation of some novel disazo indole dyes, J. Mol. Liq. 199 (2014) 227–236. https://doi.org/10.1016/j.molliq.2014.09.019.

[20] Ç. Karabacak Atay, Y. Kara, M. Gökalp, I. Kara, T. Tilki, F. Karci, Disazo dyes containing pyrazole and indole moieties: Synthesis, characterization, absorption characteristics, theoretical calculations, structural and electronic properties, J. Mol. Liq. 215 (2016) 647–655. https://doi.org/10.1016/j.molliq.2016.01.031.

[21] Ç. Karabacak Atay, M. Gökalp, S. Özdemir Kart, T. Tilki, Mono azo dyes derived from 5-nitroanthranilic acid: Synthesis, absorption properties and DFT calculations, J. Mol. Stuct. 1141 (2017) 237–244. https://doi.org/10.1016/j.molstruc.2017.03.107.

[22] N. Sener, A. Bayrakdar, H.H. Kart, I. Sener, A combined experimental and DFT investigation of disazo dye having pyrazole skeleton, J. Mol. Struct. 1129 (2017) 222–230. https://doi.org/10.1016/j.molstruc.2016.09.082.

[23] F. Yıldırım, A. Demirçalı, F. Karcı, A. Bayrakdar, P. Tunay Taşlı, H.H. Kart, New coumarin-based disperse disazo dyes: Synthesis, spectroscopic properties and theoretical calculations, J. Mol. Liq. 223 (2016) 557–565. https://doi.org/10.1016/j.molliq.2016.08.008.

[24] J.B. Foresman, A.E. Frisch, Exploring chemistry with electronic structure methods, Gaussian Inc., 1996.

[25] M.J. Frisch, et al., Gaussian 09, Revision A.1, Gaussian, Inc., Wallingford CT, 2009.

[26] M.H. Jamroz, Vibrational Energy Distribution Analysis, VEDA 4 Program, Warsaw, 2004.

[27] A.P. Scott, L. Radon, Harmonic Vibrational Frequencies: An Evaluation of Hartree–Fock, Møller–Plesset, Quadratic Configuration Interaction, Density Functional Theory, and Semiempirical Scale Factors, J. Phys. Chem. 100 (1996) 16502–16513, https://doi.org/10.1021/jp960976r.

[28] K. Fukui, Role of Frontier Orbitals in Chemical Reactions, Science 218 (1982) 747–754, https://doi.org/10.1126/science.218.4574.747.